S1 Some key concepts used in the study

Effective radiative forcing: Radiative forcing has been variously defined, but the core definition involves the net change in the energy balance of the earth system due to imposed perturbations (Myhre et al., 2013), defined positive downward, before there is substantial change in global mean surface temperatures. Radiative forcing could be a powerful metric if the equilibrium temperature were to depend only on the estimated radiative forcing and is independent of the forcing agents. Several different operational definitions of radiative forcing exist, each one with its advantages and limitations (Gregory et al., 2004; Hansen et al., 2005; Ban-Weiss et al., 2012; Myhre et al., 2013; Modak et al., 2018). The 'instantaneous radiative forcing' is defined as the instantaneous change (with no change to the climate state) in net radiative flux at TOA or at the climatological tropopause to an imposed change (Myhre et al., 2013). As the adjustment time scale of the stratosphere differs from that of the troposphere and surface, a slightly modified definition of radiative forcing called the 'stratosphere-adjusted' radiative forcing was introduced. Under this definition, stratospheric temperatures are allowed to relax to a steady state, while tropospheric temperatures are held constant, before estimating the TOA energy imbalance. In this case, the adjustment of the stratosphere is considered as a component of forcing rather than response. Later, it was found that in the case of some forcing agents such as black carbon aerosols, a layer of troposphere could experience large warming on a very short timescale and hence it was argued that the adjustment of the tropospheric layer should be considered as a component of forcing, rather than response in such cases (Hansen et al., 2005). This led to a new definition of radiative forcing called the 'effective radiative forcing' which estimates the TOA radiative flux after the stratosphere, troposphere and land surface have adjusted (Hansen et al., 2005; Myhre et al., 2013). The effective radiative forcing has been identified as a better predictor of equilibrium surface temperature change than the instantaneous and stratosphere-adjusted radiative forcing (Hansen et al., 2005; Ban-Weiss et al., 2012; Myhre et al., 2013).

There are now at least three specific operational methods of estimation of "effective radiative forcing" that can be applied to step function changes in radiative forcing agents, all of them consistent with the IPCC (Myhre et al., 2013) general definition of 'the radiative forcing with rapid adjustments accounted for". These are: the "prescribed-SST method" (Hansen et al., 2005; Bala et al., 2010), the 'regression method' (Gregory et al., 2004; Gregory and Webb 2008), and the "two-point method" (Modak et al., 2018; Duan et al., 2018). We discuss these three methods below but also note that recently Tang et al. (2019) discussed six different methods of estimating the effective radiative forcing. The other three methods involve using exponential and polynomial fits instead linear regression and using radiative kernels to correct for the land surface response.

The prescribed-SST method (Hansen et al., 2005; Bala et al., 2010) estimates the effective radiative forcing as the TOA net radiative flux change upon the introduction of the forcing in a simulation where sea surface temperatures and sea-ice concentration are prescribed. Because land-surface temperatures are allowed to evolve in the prescribed-SST simulations, there

is some global mean temperature change, and the radiative effects of this temperature change are included as part of the forcing in the prescribed-SST method.

In the regression method (Gregory et al., 2004; Gregory and Webb 2008), the change in TOA net radiative flux (ΔN) for an abrupt change in the forcing agent is regressed against the transient global mean surface temperature response (ΔT) in a slab ocean or coupled simulation. The y-intercept (for $\Delta T = 0$) gives an estimate of the radiative forcing and slope of the regression line is the climate feedback parameter. Forster et al., (2016) recommends the use of the prescribed-SST method over the regression method for radiative forcing estimates because the prescribed-SST simulations can be extended to any length of time to achieve an adequately small standard error of the estimate. The regression method (Gregory et al., 2004; Gregory and Webb, 2008) has the advantage of being applicable to transient simulations with full dynamical ocean models, and further avoids making assumptions that the effective radiative forcing would be the same with and without specification of sea-surface temperatures. The regression method requires larger ensembles to reduce the standard error of the estimate.

The two-point method (Modak et al., 2018; Duan et al., 2018) attempts to improve on the prescribed-SST method by correcting for the global mean temperature change that occurs in prescribed-SST simulations due to changes in land surface temperatures and is most suitable to circumstances when equilibrium climate change can be determined, such as in climate models with a slab ocean model representation of the ocean. Let ΔN_{SST} and ΔN_{SOM} represent the equilibrium top-of-atmosphere net downward radiative flux changes in prescribed SST and slab-ocean-model simulations, respectively. Further, let ΔT_{SST} and ΔT_{SOM} represent the equilibrium global mean near-surface temperature changes for prescribed SST and slab-ocean-model simulations, respectively. In this framework, the radiative forcing (F), and the climate-feedback parameter (λ) are defined as:

$$F = \Delta N_{SST} + \lambda\, \Delta T_{SST} \tag{1}$$

and

$$\lambda = (\Delta N_{SST} - \Delta N_{SOM}) / (\Delta T_{SOM} - \Delta T_{SST}) \tag{2}$$

This two-point method has the advantage over prescribed-SST method, in that the equilibrium climate change from a forcing (ΔT_{SOM}) is equal to F / λ when the slab ocean simulations have reached equilibrium ($\Delta N_{SOM} = 0$). As with the prescribed-SST method, standard errors of the estimates of these values can be reduced arbitrarily by increasing the number of simulated years, but with this method errors of the estimates depend on uncertainties in global means results for both the prescribed-SST and slab-ocean-model simulations. In this study, when presenting results for radiative forcing, the climate-feedback parameter and efficacy (see below) we estimate these values using this two-point method.

Fast adjustments: According to the above discussion on radiative forcing and in the context of the forcing-response framework (Sherwood et al., 2015), the difference between the instantaneous radiative forcing and the effective radiative forcing is attributed to 'fast adjustments'. What counts as a fast adjustment depends on which definition of 'effective radiative forcing' is used. For example, in the prescribed-SST definition, changes in the stratosphere, troposphere and land surface temperature (and resulting change in global mean temperature) are considered as part of the fast adjustment. In the regression and two-point methods, fast changes in the stratosphere, troposphere, land-surface and sea surface temperature patterns (but not change in global mean temperature) are considered as part of the fast adjustment. These fast adjustments could include large changes in tropospheric temperature, clouds, water vapor and precipitation (Bala et al., 2010; Myhre et al., 2018).

Efficacy: Even when the effective radiative forcing is used for estimating the equilibrium response, it has been found that different forcing agents could result in different responses (Hansen et al., 2005; Modak et al., 2016; Modak et al., 2018). This undermines the fundamental rationale for using the radiative forcing concept. To account for these differing climate responses, Hansen et al., (2005) proposed the concept of 'efficacy' which compares the effects of a forcing agent to that of CO_2. 'Efficacy' is defined as the ratio of the equilibrium global mean temperature change per unit effective radiative forcing by a forcing agent relative to the equilibrium temperature change per unit CO_2 forcing from the same initial climate state. Efficacy values will vary depending on the definition of effective radiative forcing being applied (Modak et al., 2018). Here, we apply the two-point method in our reported results. If λ_{SAI} and λ_{CO2} are the climate feedback parameters calculated for step-function changes in stratospheric aerosol concentrations and CO_2 concentrations, respectively, calculated from the two-point method, 'efficacy' of the stratospheric aerosol injection radiative forcing (e_{SAI}) can be defined as

$$e_{SAI} = \lambda_{CO2} / \lambda_{SAI} \tag{3}$$

Because the equilibrium temperature change (ΔT) is F / λ, a value for $e_{SAI} > 1$ would mean that for the same effective radiative forcings, stratospheric aerosols would cause a large equilibrium near-surface temperature change than would CO_2.

Efficiency of aerosols: In-order to quantify the effect of aerosols on surface cooling, we define 'efficiency' of stratospheric sulfate aerosol as the change in surface temperature per additional Tg-S resident in the stratosphere (1 Tg-S = 1 Mt-S = 2.0 Mt-SO_2 = 3.0 Mt-SO_4). This is different from the definitions used in recent studies (e.g. Tilmes et al., 2017) where efficiency is defined as the surface temperature change per unit Mt of S or unit Mt of SO_2 injected into the stratosphere.

References

Bala, G., Caldeira, K., and Nemani, R.: Fast versus slow response in climate change: implications for the global hydrological cycle, Clim. Dyn., 35, 423-434, doi:10.1007/s00382-00009-00583-y, 2010.

5   Ban-Weiss, G. A., Cao, L., Bala, G., and Caldeira, K.: Dependence of climate forcing and response on the altitude of black carbon aerosols, Clim. Dyn., 38, 897-911, https ://doi.org/10.1007/s00382-011-1052-y, 2012.

Duan, L., Cao, L., Bala, G., and Caldeira, K.: Comparison of the fast and slow climate response to three radiation management geoengineering schemes, J. Geophys. Res. Atmos., 123, 11980-12001, https://doi.org/10.1029/2018JD029034, 2018.

Forster, P. M., Richardson, T., Maycock, A. C., Smith, C. J., Samset, B. H., Myhre, G., Andrews, T., Pincus, R., Schulz, M.,
10   Recommendations for diagnosing effective radiative forcing from climate models for CMIP6, J. Geophys. Res. Atmos., 121, 12460-12475, 2016.

Gregory, J. M., Ingram, W. J., Palmer, M. A., Jones, G. S., Stott, P. A., Thorpe, R. B., Lowe, J. A., Johns, T. C., and Williams, K. D.: A new method for diagnosing radiative forcing and climate sensitivity, Geophys. Res. Lett., 31, L03205, doi:10.1029/2003GL018747, 2004.

15   Gregory, J. M., Webb, M. J.: Tropospheric adjustment induces a cloud component in CO_2 forcing, J. Climate, 21, 58-71, doi:10.1175/2007JCLI1834.1, 2008.

Hansen, J., Sato, M., Ruedy, R., Nazarenko, L., Lacis, A., Schmidt, G. A., Russell, G., Aleinov, I., Bauer, M., Bauer, S., Bell, N., Cairns, B., Canuto, V., Chandler, M., Cheng, Y., Del Genio, A., Faluvegi, G., Fleming, E., Friend, A., Hall, T., Jackman, C., Kelley, M., Kiang, N., Koch, D., Lean, J., Lerner, J., Lo, K., Menon, S., Miller, R., Minnis, P., Novakov, T., Oinas, V.,
20   Perlwitz, J., Perlwitz, J., Rind, D., Romanou, A., Shindell, D., Stone, P., Sun, S., Tausnev, N., Thresher, D., Wielicki, B., Wong, T., Yao, M. and Zhang, S.: Efficacy of climate forcings, J. Geophys. Res. Atmos., 110, 110, D18104, doi:10.1029/2005JD005776, 2005.

Modak, A., Bala, G., Cao, L., and Caldeira, K.: Why must a solar forcing be larger than a CO_2 forcing to cause the same global mean surface temperature change? Environ. Res. Lett., 11(4), 044013, http://doi.org/10.1088/1748-9326/11/4/044013, 2016.

25   Modak, A., Bala, G., Caldeira, K., and Cao, L.: Does shortwave absorption by methane influence its effectiveness? Clim. Dyn., 51(9-10), 3653-3672, http://doi.org/10.1007/s00382-018-4102-x, 2018.

Myhre, G., Shindell, D., Bréon, F.-M., Collins, W., Fuglestvedt, J., Huang, J., Koch, D., Lamarque, J.-F., Lee, D., Mendoza, B., Nakajima, T., Robock, A., Stephens, G., Takemura, T. and Zhang, H.: Anthropogenic and natural radiative forcing, in

Climate Change 2013: The Physical Science Basis. Contribution of Working Group I to the Fifth Assessment Report of the Intergovernmental Panel on Climate Change, edited by T. F. Stocker, D. Qin, G.-K. Plattner, M. Tignor, S. K. Allen, J. Doschung, A. Nauels, Y. Xia, V. Bex, and P. M. Midgley, pp. 659–740, Cambridge University Press, Cambridge, UK., 2013.

Myhre, G., Kramer, R. J., Smith, C. J., Hodnebrog, Ø., Forster, P., Soden, B. J., Samset, B. H., Stjern, C. W., Andrews, T., Boucher, O., Faluvegi, G., Fläschner, D., Kasoar, M., Kirkevåg, A., Lamarque, J.-F., Olivié, D., Richardson, T., Shindell, D., Stier, P., Takemura, T., Voulgarakis, A. and Watson-Parris, D.: Quantifying the Importance of Rapid Adjustments for Global Precipitation Changes, Geophys. Res. Lett., 45(20), 11399-11405, doi:10.1029/2018GL079474, 2018.

Sherwood, S. C., Bony, S., Boucher, O., Bretherton, C., Forster, P. M., Gregory, J. M. and Stevens, B.: Adjustments in the forcing-feedback framework for understanding climate change, Bull. Am. Meteorol. Soc., 96(2), 217–228, doi:10.1175/BAMS-D-13-00167.1, 2015.

Tang, T., Shindell, D. T., Faluvegi, G., Myhre, G., Olivié, D., Voulgarakis, A., Kasoar, M., Andrews, T., Boucher, O., Forster, P. M., Hodnebrog, Ø., Iversen, T., Kirkevåg, A., Lamarque, J. F., Richardson, T. B., Samset, B. H., Stjern, C. W., Takemura, T. and Smith, C. J.: Comparison of Effective Radiative Forcing Calculations using Multiple Methods, Drivers, and Models, 124, https://doi.org/10.1029/2018JD030188.

Tilmes, S., Richter, J. H., Mills, M. J., Kravitz, B., MacMartin, D. G., Vitt, F., Tribbia, J. J. and Lamarque, J.-F.: Sensitivity of Aerosol Distribution and Climate Response to Stratospheric SO_2 Injection Locations, J. Geophys. Res. Atmos., 122(23), 12591-12615, doi:10.1002/2017JD026888, 2017.
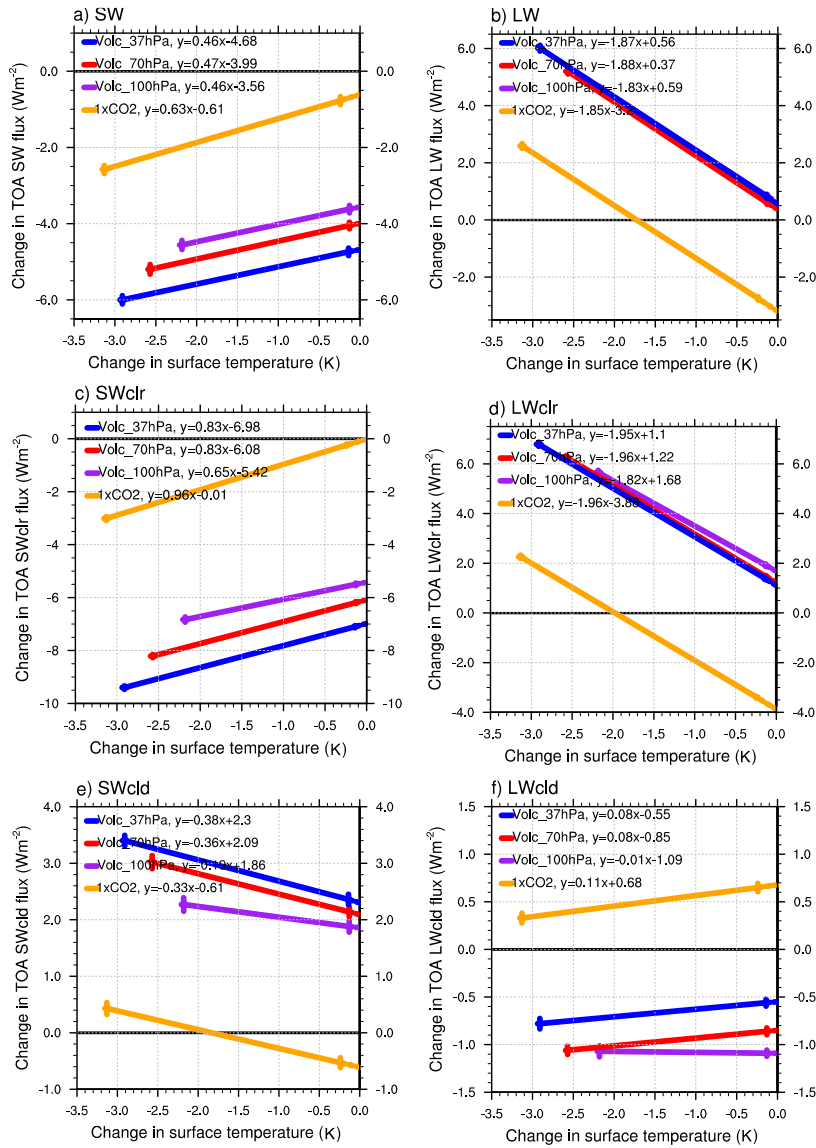
Figure S1: The two-point method for estimating the components of radiative forcing and feedback parameter (Sect. S1). Change in global and annual mean surface temperature and TOA radiative flux components from the slab ocean (points on the left) and prescribed SST (points on the right) runs relative to the corresponding 2XCO2 simulation. The feedback parameter (slope of the lines) and the corrected radiative forcing (intercept on the y-axis on the right) for CO_2 change (1XCO2-2XCO2) and all geoengineering experiments can be inferred from the linear regression relationships shown in the figure legends. Horizontal and vertical bars show 2 standard errors of the annual mean differences in surface temperature and radiative forcing relative to 2XCO2 experiment, respectively. The standard errors are estimated using 30 annual means for prescribed-SST simulations and 60 annual means for slab ocean simulations.

6
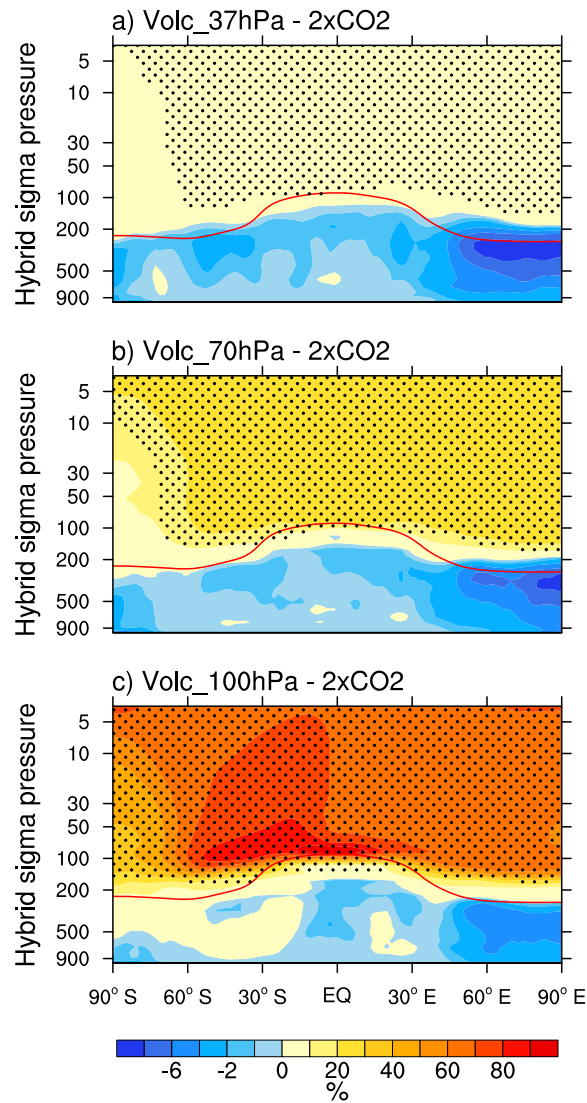
Figure S2: Percentage change in zonal mean specific humidity in the prescribed SST version of the stratospheric aerosol experiments relative to the prescribed SST version of the 2XCO2 experiment. The hatched area in the plot shows the regions where the changes are significant at 5% significance level. Significance level is estimated using Students t-test using 30 annual means of the experiments. The red solid line shows the tropopause in the 1XCO2 experiment. The warming of the tropical tropopause layer in the Volc_100hPa case (Fig. S5) is associated with an increase in humidity in the stratosphere by enhanced transport of water vapor from troposphere. Large increases in specific humidity are simulated when the volcanic aerosols are prescribed in the lower levels of the stratosphere.

a) Total cloud

b) High cloud
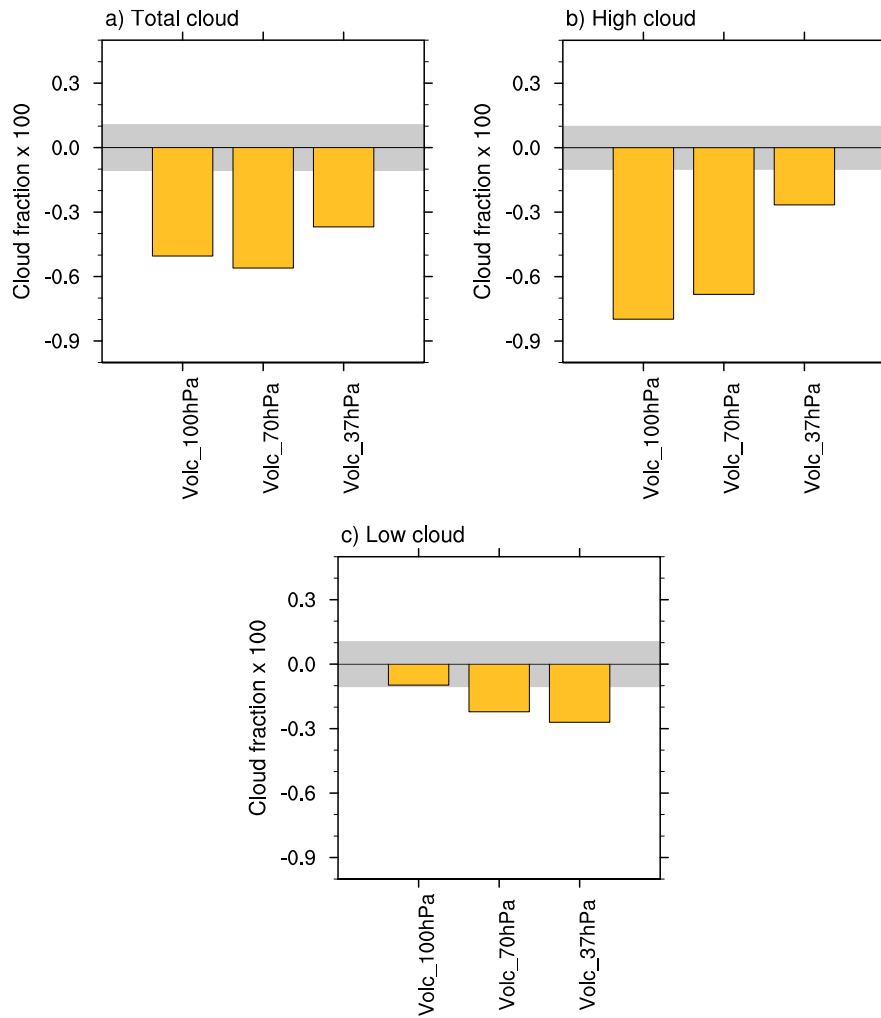
c) Low cloud

Figure S3: Changes in global and annual mean cloud fraction for a) total b) high and c) low clouds relative to the 2XCO2 experiment. These are fast cloud adjustments as these changes are estimated from the prescribed-SST experiments. The width of the grey shaded region represents two standard deviations calculated from 30 annual means from the 2XCO2 experiment. There is an overall reduction in total cloud fraction in the stratospheric aerosol experiments mainly contributed by the reduction in high clouds. For high clouds, a large sensitivity to the height of the aerosols is simulated. The upper tropospheric warming (Fig. S4 and S5) associated with radiative heating in the aerosol layer leads to a reduction in high clouds. Also, as the upper troposphere warms (Fig. S5), the stability of the troposphere increases which reduces the water vapor transport to the upper troposphere reducing the probability of ice-supersaturation (Visioni, 2018) and thereby causing a reduction in high clouds. A reduction is low clouds is associated with a reduction in solar absorption in the upper troposphere (Modak et al., 2016). The upper tropospheric warming in the Volc_100hPa (Fig. S5) case partially offsets this effect and hence the magnitude of the reduction is less in the Volc_100hPa case.

8
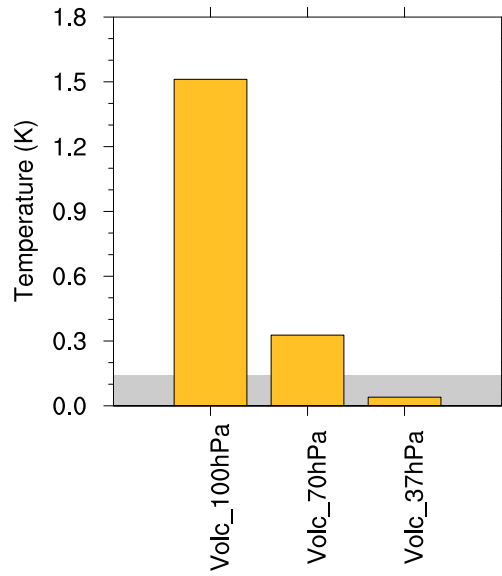
Figure S4: Changes in global and annual mean upper atmospheric temperature (mass weighted average between 100 hPa and 200 hPa) in the prescribed SST simulations relative to the 2XCO2 experiment. The width of the grey shaded region represents one standard deviation calculated from 30 annual means from the 2XCO2 experiment. The absorption of SW and LW radiation by aerosols causes an increase in temperature in the stratosphere (Fig. S5). Along with the stratospheric temperature changes, the upper troposphere also warms slightly in the stratospheric aerosol experiments. This upper tropospheric warming depends on the magnitude of radiative heating by the prescribed aerosols and the distance of the warmer aerosol layer from the tropopause. The upper tropospheric temperature is maximum when the aerosols are prescribed at the lower levels of the stratosphere (Fig. S5) and decreases as the aerosol layer is moved up.
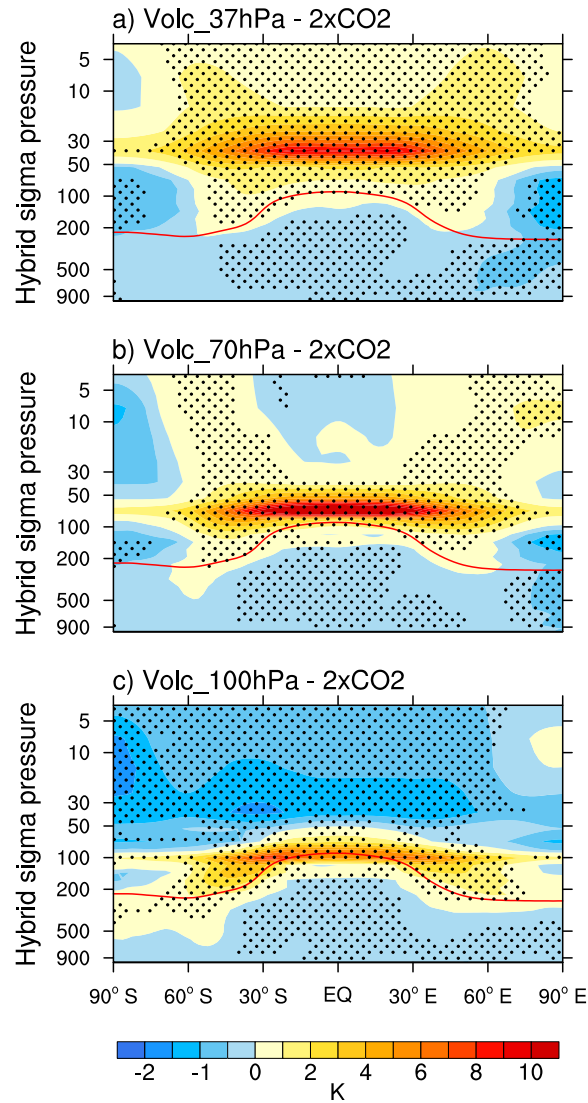
Figure S5: The changes in global and annual mean of zonally averaged temperature in the prescribed SST version of the stratospheric aerosol simulations relative to the 2XCO2 experiment. The red solid line shows the tropopause in the 1XCO2 experiment. In all cases, radiative heating in the layers where aerosols are prescribed can be clearly seen. The hatched area in the plot shows the regions where the changes are significant at 5% significance level. Significance level is estimated using Students t-test from calculated from 30 annual means of the experiments.
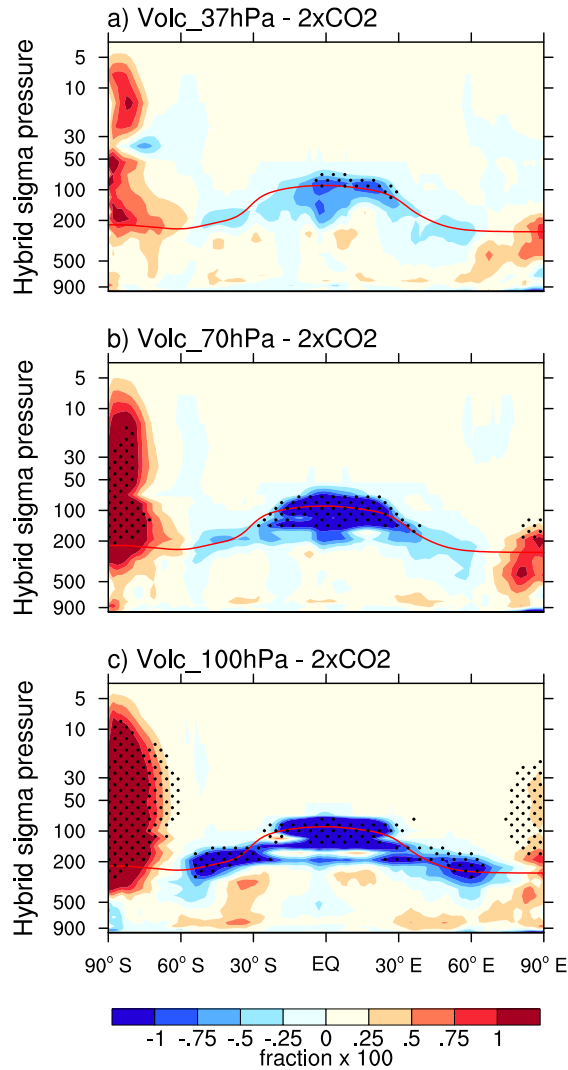
Figure S6: Changes in zonal mean clouds in the prescribed SST simulations relative to the 2XCO2 experiment. The red solid line shows the tropopause in the 1XCO2 experiment. The prominent feature is the reduction in tropical upper level clouds which is related to the radiative heating due to the prescribed aerosols (Fig. S5). Also, as the upper troposphere warms, the stability of the troposphere increases leading to a reduction in water transport to the upper troposphere thereby reducing the probability of ice-supersaturation (Visioni et al., 2018) and resulting in reduction of high clouds. The increased cloudiness simulated in the polar stratosphere is consistent with Boucher et al. (2017), which they attribute to the transport of additional water vapor entering stratosphere to the poles. The hatched area in the plot shows the regions where the changes are significant at 5% significance level. Significance level is estimated using Students t-test from calculated from 30 annual means of the experiments.

11
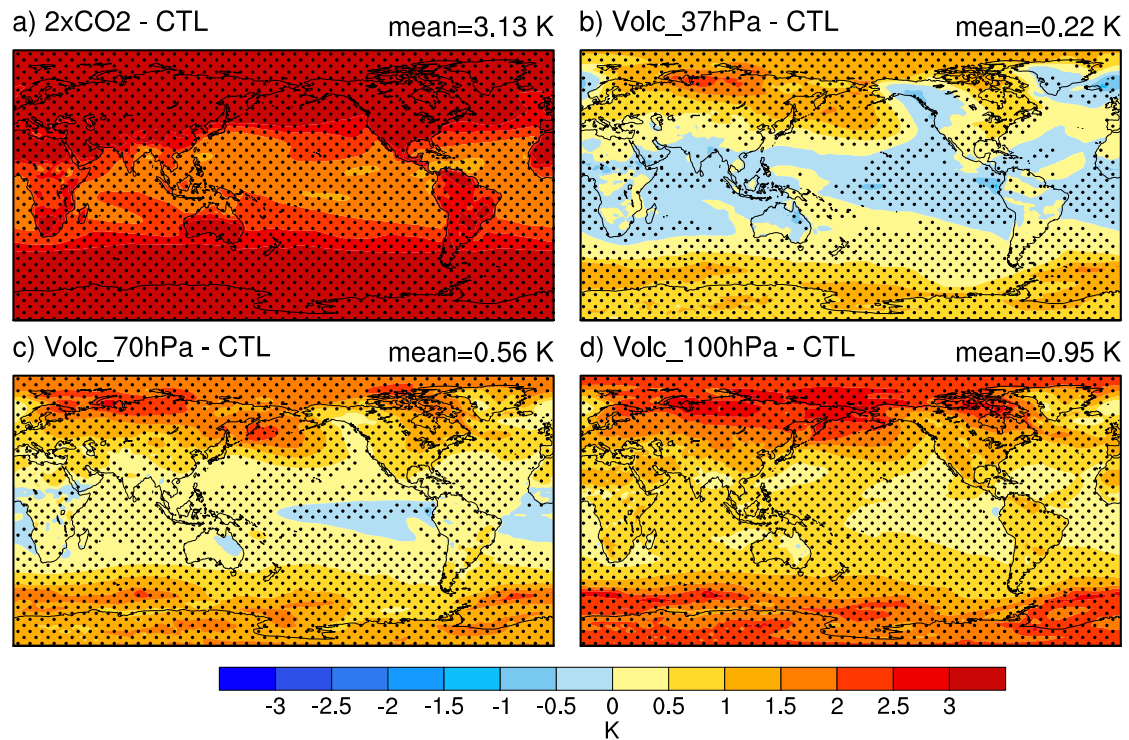
Figure S7: The spatial pattern of changes in surface temperature relative to the 1XCO2 experiment. The hatched areas show the regions where the changes are significant at the 5% significance level. Significance level is estimated using Students t-test from 60 annual means of the experiments. Global mean value of the changes in each experiment is shown at the top left of each panel.
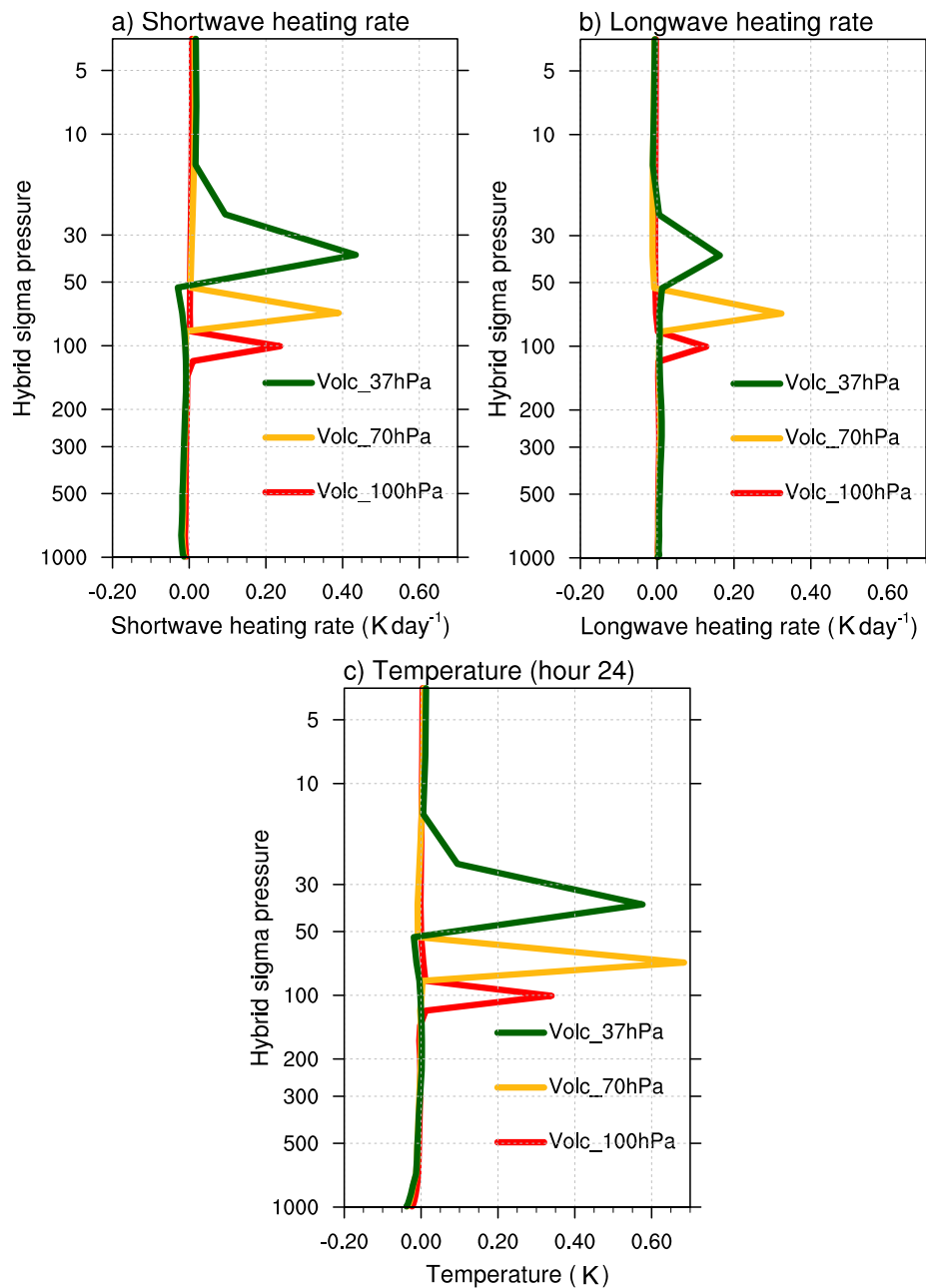
Figure S8: The daily mean (a) shortwave and (b) longwave heating rates change and (c) temperature change for the stratospheric sulfate experiments from the 1-day runs relative to the 2XCO2 experiment. Lines are linear interpolations between layer midpoint values.

a) Direct (Volc_100hPa - 2xCO2) mean=-9.45 W.m^{-2}

-20 -16 -12 -8 -4 0 4 8 12 16 20   W.m^{-2}
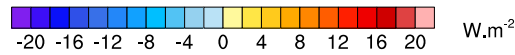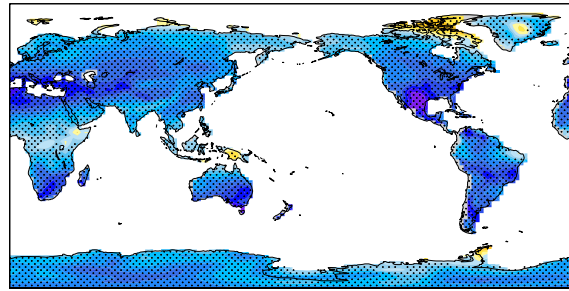
b) Diffuse (Volc_100hPa - 2xCO2) mean=8.09 W.m^{-2}

-20 -16 -12 -8 -4 0 4 8 12 16 20   W.m^{-2}

c) Cloud cover (2xCO2)

0   0.1 0.2 0.3 0.4 0.5 0.6 0.7 0.8 0.9   1   fraction
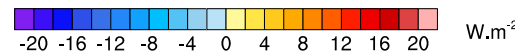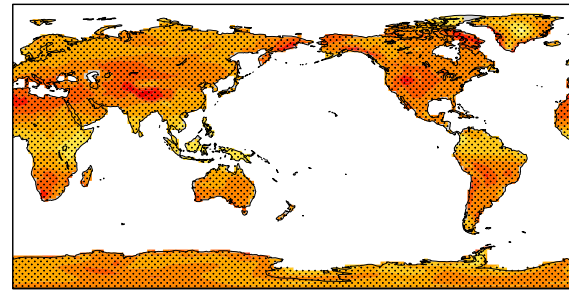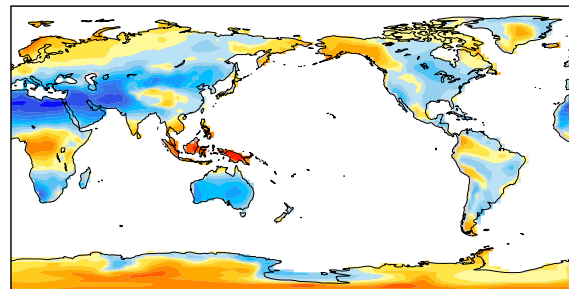
Figure S9: The spatial pattern of changes, relative to the 2XCO2 experiment, in direct (top panel) and diffuse (middle panel) radiation for the cases where volcanic aerosols are prescribed at 100 hPa. The hatched area in the plot shows the regions where the changes are significant at the 5% significance level. Significance level is estimated using Students t-test from 60 annual means of the experiments. The vertically integrated total cloud cover for the 2XCO2 case is shown in the bottom panel.

Table S1. The net radiative forcing and its components relative to the 2XCO2 experiment estimated from the two-point method (Sect. S1). The corresponding feedback parameters are also shown. The uncertainties are given by standard errors which is estimated using 30 annual means of the differences from the 2XCO2 experiment.

	1XCO2	Volc_100hPa	Volc_70hPa	Volc_37hPa
RF	-3.82±0.09	-2.97±0.11	-3.62±0.09	-4.12±0.11
RF_{SW}	-0.61±0.11	-3.56±0.10	-3.99±0.09	-4.68±0.10
RF_{LW}	-3.20±0.06	0.59±0.06	0.37±0.06	0.56±0.07
RF_{SWclr}	-0.01±0.04	-5.42±0.05	-6.08±0.04	-6.98±0.04
RF_{SWcld}	-0.61±0.09	1.86±0.10	2.09±0.09	2.30±0.09
RF_{LWclr}	-3.88±0.07	1.68±0.10	1.22±0.08	1.10±0.09
RF_{LWcld}	0.68±0.04	-1.09±0.03	-0.85±0.04	-0.55±0.04
λ	1.22±0.05	1.37±0.09	1.41±0.07	1.42±0.06
λ_{SW}	-0.63±0.05	-0.46±0.08	-0.47±0.06	-0.46±0.05
λ_{LW}	1.85±0.04	1.83±0.06	1.88±0.05	1.87±0.05
λ_{SWclr}	-0.96±0.03	-0.65±0.05	-0.83±0.03	-0.83±0.03
λ_{SWcld}	0.33±0.05	0.19±0.08	0.36±0.06	0.38±0.05
λ_{LWclr}	1.96±0.07	1.82±0.10	1.96±0.08	1.95±0.09
λ_{LWcld}	-0.11±0.04	0.01±0.03	-0.08±0.04	-0.08±0.04